Distribution functions of a radially excited pion

Zhen-Ni Xu

Universidad de Huelva

28/05/2025, at ECT*

In collaboration with: José Rodríguez Quintero, Craig D. Roberts

Ground-state pion

- The pion is a bound state seeded by a light quark and light anti-quark, *e.g.*, $\pi^+ = u\bar{d}$.
- Nature's most fundamental Nambu-Goldstone boson

Ground-state pion

- The pion is a bound state seeded by a light quark and light anti-quark, *e.g.*, $\pi^+ = u\bar{d}$.
- Nature's most fundamental Nambu-Goldstone boson
- Gell-Mann–Oakes–Renner relation (GMOR)

$$f_\pi m_\pi^2 = (m_u^\zeta + m_d^\zeta) r_\pi^\zeta \,, \qquad (1)$$

f_π remains nonzero as Higgs boson couplings are removed: $f_\pi^0 \approx 0.088\,\text{GeV}$. [Gasser:1983yg]

$$m_\pi^0 = 0$$

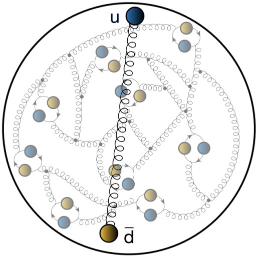

Figure: Z.-F. Cui et al.,2020 Chinese Phys. C 44 083102

Ground-state pion

- Poincaré-covariant amplitude

$$\Gamma_\pi(k;P) = \gamma_5\,[iE_\pi(k;P) + \gamma\cdot PF_\pi(k;P) \\ +\gamma\cdot k k\cdot PG_\pi(k;P) + \sigma_{\mu\nu}k_\mu P_\nu H_\pi(k;P)]\ , \quad (2)$$

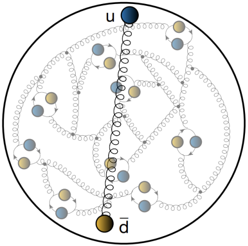

Figure: Z.-F. Cui et al.,2020 Chinese Phys. C 44 083102

Ground-state pion

- Poincaré-covariant amplitude

$$\Gamma_\pi(k;P) = \gamma_5 \left[iE_\pi(k;P) + \gamma \cdot P F_\pi(k;P) + \gamma \cdot k k \cdot P G_\pi(k;P) + \sigma_{\mu\nu} k_\mu P_\nu H_\pi(k;P) \right] , \quad (2)$$

- Goldberger-Treiman relation:

$$f_\pi^0 E_\pi^0(k,0;\zeta) = B^0(k;\zeta) . \quad (3)$$

- $B^0(k;\zeta)$: scalar piece of the dressed quark self-energy
- crucial link between the pseudoscalar two-body and quark one-body problems
- most fundamental expression of Goldstone's theorem in QCD

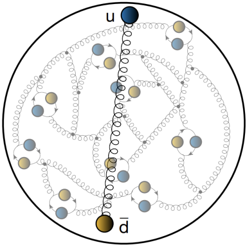

Figure: Z.-F. Cui et al.,2020 Chinese Phys. C 44 083102

Radial excitation of π

- Far less is known about pion's radially excited counterpart, π_1
- GMOR relation

$$f_\pi m_\pi^2 = (m_u^\zeta + m_d^\zeta) r_\pi^\zeta \,, \tag{4}$$

Radial excitation of π

- Far less is known about pion's radially excited counterpart, π_1
- GMOR relation

$$f_\pi m_\pi^2 = (m_u^\zeta + m_d^\zeta) r_\pi^\zeta \,, \tag{4}$$

- More general identity, valid for every pseudoscalar meson:

$$f_{\pi_n} m_{\pi_n}^2 = (m_u^\zeta + m_d^\zeta) r_{\pi_n}^\zeta \,, \tag{5}$$

π_n: radial excitation n of the pion ground-state π_0.

C. A. Dominguez, Phys. Rev. D 15, 1350

A. Höll et al., Phys. Rev. D 15, 1350

Radial excitation of π

- Far less is known about pion's radially excited counterpart, π_1
- GMOR relation

$$f_\pi m_\pi^2 = (m_u^\zeta + m_d^\zeta) r_\pi^\zeta \,, \tag{4}$$

- More general identity, valid for every pseudoscalar meson:

$$f_{\pi_n} m_{\pi_n}^2 = (m_u^\zeta + m_d^\zeta) r_{\pi_n}^\zeta \,, \tag{5}$$

π_n: radial excitation n of the pion ground-state π_0.
C. A. Dominguez, Phys. Rev. D 15, 1350

A. Höll et al., Phys. Rev. D 15, 1350

  - Calculations and experiment show that pion radial excitations exist and are **very massive**
  - **In the chiral limit**:

$$\forall n \geq 1 \mid f_{\pi_n}^0 \equiv 0 \,. \tag{6}$$

  An array of calculations at physical quark current masses indicate $|f_{\pi_1}| < 10\,\mathrm{MeV}$. **Our prediction** is $f_{\pi_1} = 7.8(5)\,\mathrm{MeV}$.

Dyson-Schwinger Equations

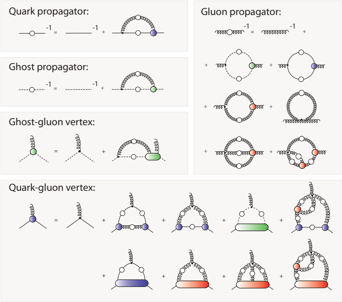

- an infinite tower of coupled integral equations which involve Green functions of all orders.
- are nonperturbative in nature since Green functions all are fully dressed.

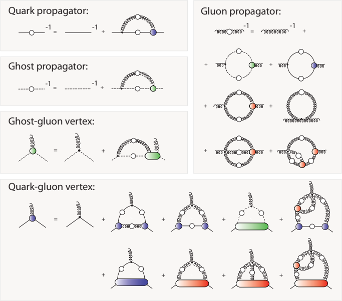

- an infinite tower of coupled integral equations which involve Green functions of all orders.
- are nonperturbative in nature since Green functions all are fully dressed.

- Quark propagator: gap equation

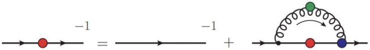

$$S_g^{-1}(k) = i\gamma \cdot k + m_g + \Sigma_g(k),$$

$$\Sigma_g(k) = \int dq\, 4\pi\alpha D_{\mu\nu}(l)\gamma_\mu \frac{\lambda^a}{2} S(q)\Gamma^g_\nu(q,k)\frac{\lambda^a}{2}$$

Dyson-Schwinger Equations

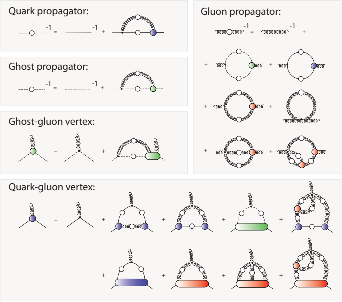

- an infinite tower of coupled integral equations which involve Green functions of all orders.
- are nonperturbative in nature since Green functions all are fully dressed.

- Quark propagator: gap equation

$$S_g^{-1}(k) = i\gamma \cdot k + m_g + \Sigma_g(k),$$

$$\Sigma_g(k) = \int dq\, 4\pi\alpha D_{\mu\nu}(l)\gamma_\mu \frac{\lambda^a}{2} S(q)\Gamma_\nu^g(q,k)\frac{\lambda^a}{2}$$

- Bethe-Sapleter equation

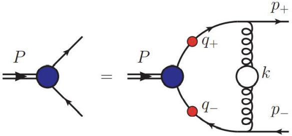

$$\Gamma^{gh}_{H\alpha\beta}(k;P) = \int_{dq} K^{(2)}_{\alpha\alpha',\beta\beta'}\chi^{gh}_{H\alpha'\beta'}(q,P)$$

DSE: quark+gluon vertex

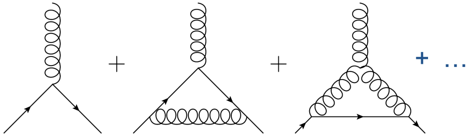

Figure: Quark+gluon vertex

Rainbow-Ladder truncation

- Rainbow truncation

$$4\pi\alpha D_{\mu\nu}(l)\Gamma^{g}_{\nu}(q,k) \to \mathcal{G}_{\mu\nu}(l)\gamma_{\nu}$$

Munczek H J 1995 Phys. Rev. D 52 4736

Bender A et al., Phys. Lett. B 380 7

- Ladder truncation

$$\mathcal{K}^{rs}_{tu} = \mathcal{G}_{\mu\nu}(l)[i\gamma_{\mu}\frac{\lambda^{a}}{2}]_{ts}[i\gamma_{\nu}\frac{\lambda^{a}}{2}]_{ru}$$

DSE: quark+gluon vertex

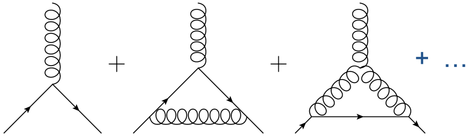

Figure: Quark+gluon vertex

Rainbow-Ladder truncation

- Rainbow truncation

$$4\pi\alpha D_{\mu\nu}(l)\Gamma^g_\nu(q,k) \to \mathcal{G}_{\mu\nu}(l)\gamma_\nu$$

Munczek H J 1995 Phys. Rev. D 52 4736

Bender A et al., Phys. Lett. B 380 7

- Ladder truncation

$$\mathcal{K}^{rs}_{tu} = \mathcal{G}_{\mu\nu}(l)[i\gamma_\mu \frac{\lambda^a}{2}]_{ts}[i\gamma_\nu \frac{\lambda^a}{2}]_{ru}$$

- serves well for ground-state hadrons with little rest-frame orbital angular momentum between the dressed valence constituents.

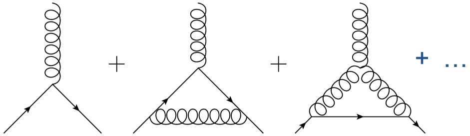

Figure: Quark+gluon vertex

Rainbow-Ladder truncation

- Rainbow truncation

$$4\pi\alpha D_{\mu\nu}(l)\Gamma^{g}_{\nu}(q,k) \to \mathcal{G}_{\mu\nu}(l)\gamma_{\nu}$$

Munczek H J 1995 Phys. Rev. D 52 4736

Bender A et al., Phys. Lett. B 380 7

- Ladder truncation

$$\mathcal{K}^{rs}_{tu} = \mathcal{G}_{\mu\nu}(l)[i\gamma_{\mu}\frac{\lambda^{a}}{2}]_{ts}[i\gamma_{\nu}\frac{\lambda^{a}}{2}]_{ru}$$

- serves well for ground-state hadrons with little rest-frame orbital angular momentum between the dressed valence constituents.
- fails for other systems: being omission of those structures

  Si-xue Qin et al., Phys. Rev. C 85, 035202

DSE: quark+gluon vertex

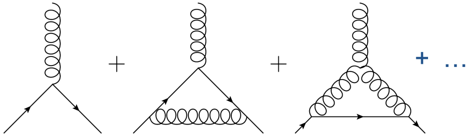

Figure: Quark+gluon vertex

Rainbow-Ladder truncation

- Rainbow truncation

$$4\pi\alpha D_{\mu\nu}(l)\Gamma^{g}_{\nu}(q,k) \to \mathcal{G}_{\mu\nu}(l)\gamma_{\nu}$$

Munczek H J 1995 Phys. Rev. D 52 4736

Bender A et al., Phys. Lett. B 380 7

- Ladder truncation

$$\mathcal{K}^{rs}_{tu} = \mathcal{G}_{\mu\nu}(l)[i\gamma_{\mu}\frac{\lambda^a}{2}]_{ts}[i\gamma_{\nu}\frac{\lambda^a}{2}]_{ru}$$

- serves well for ground-state hadrons with little rest-frame orbital angular momentum between the dressed valence constituents.
- fails for other systems: being omission of those structures

  Si-xue Qin et al., Phys. Rev. C 85, 035202
- inadequate expression in the Bethe-Salpeter kernels...spin-orbit interactions

Beyond the rainbow-ladder

- Key missing components lie beyond RL

Eur. Phys. J. A (2023) 59:39
https://doi.org/10.1140/epja/s10050-023-00951-7

THE EUROPEAN PHYSICAL JOURNAL A

Letter

Bethe–Salpeter kernel and properties of strange-quark mesons

Zhen-Ni Xu[1,2], **Zhao-Qian Yao**[1,2,3], **Si-Xue Qin**[4,a], **Zhu-Fang Cui**[1,2,b], **Craig D. Roberts** [1,2,3,4,c]

[1] School of Physics, Nanjing University, Nanjing 210093, Jiangsu, China
[2] Institute for Nonperturbative Physics, Nanjing University, Nanjing 210093, Jiangsu, China
[3] European Centre for Theoretical Studies in Nuclear Physics and Related Areas, Villa Tambosi, Strada delle Tabarelle 286, 38123 Villazzano, TN, Italy
[4] Department of Physics, Chongqing University, Chongqing 401331, China

Received: 31 December 2022 / Accepted: 8 February 2023 / Published online: 4 March 2023
© The Author(s), under exclusive licence to Società Italiana di Fisica and Springer-Verlag GmbH Germany, part of Springer Nature 2023
Communicated by Andre Peshier

Abstract Focusing on the continuum meson bound-state problem, a novel method is used to calculate closed-form Bethe–Salpeter kernels that are symmetry consistent with any reasonable gluon-quark vertex, Γ_ν, and therewith deliver a Poincaré-invariant treatment of the spectrum and decay constants of the ground- and first-excited states of u, d, s mesons. The predictions include masses of as-yet unseen states and many unmeasured decay constants. The analysis reveals that a realistic, unified description of meson properties (including level orderings and mass splittings) requires a sound expression of emergent hadron mass in bound-state kernels; alternatively, that such properties may reveal much about the emergence of mass in the standard model.

at infrared momenta [4, Fig. 2.5]: $M_{u,d}(0) \simeq 0.41$ GeV, $M_s(0) \simeq 0.53$ GeV.

There are problems with the quark model position, however. One issue is the quantum mechanics description of light-quark systems in terms of a potential. Owing to the fact that light-particle annihilation and creation effects are essentially nonperturbative in QCD, it has thus for proved impossible to calculate a quantum mechanical potential between two light quarks [5–7]. Another recognises that whilst it might be possible to connect a linear potential with the Wilson area law applicable to infinitely-heavy colour-sources and -sinks [8], the associated flux tube picture [9] has neither a mathematical nor physical connection with the confinement of light quarks. In this sector, at least, confinement is more subtle, arguably

- … a novel method used to calculate closed-form Bethe-Salpeter kernels that are symmetry consistent with any reasonable gluon-quark vertex
- a realistic, unified description of meson properties requires a sound expression of EHM in bound-state kernels

EHM-improved kernel

- EHM is known to generate a large **anomalous chromomagnetic moment** (ACM) for the lighter quarks, and this ACM has a marked impact on the u, d, s meson spectrum.
  D. Binosi, et al., Phys. Rev. D 95 (2017) 031501(R).
  A. Bashir, et al., Phys. Rev. C 85 (2012) 045205.
  S.-X. Qin, et al., Chin. Phys. Lett. Express 38 (7) (2021) 071201.

EHM-improved kernel

- EHM is known to generate a large **anomalous chromomagnetic moment** (ACM) for the lighter quarks, and this ACM has a marked impact on the u, d, s meson spectrum.
  D. Binosi, et al., Phys. Rev. D 95 (2017) 031501(R).
  A. Bashir, et al., Phys. Rev. C 85 (2012) 045205.
  S.-X. Qin, et al., Chin. Phys. Lett. Express 38 (7) (2021) 071201.
- The Dirac and Pauli terms: for an on-shell fermion, the vertex can be decomposed by two form factors: S.-X. Qin, et al., Chin. Phys. Lett. Express 38 (7) (2021) 071201.

$$\Gamma_\mu(P', P) = \gamma_\mu F_1(Q^2) + \frac{i\sigma_{\mu\nu}}{2M_f} Q_\nu F_2(Q^2)$$

- The form factors express (color-)charge and (color-)magnetization densities. ACM is proportional to the Pauli term.

Beyond the rainbow-ladder

- To expand existing studies and expose novel ACM effects on mesons containing s and sbar quarks
  Zhen-Ni Xu et al., Eur. Phys. J. A 59, 39 (2023)

$$\Gamma^g_\nu(q,k) = \gamma_\nu + \tau_\nu(l), \tau_\nu(l) = \eta\kappa(l^2)\sigma_{\rho\nu} l_\rho$$
$$\kappa(l^2) = (1/\omega) exp(-l^2/\omega^2)$$

- Symmetries: constrain the kernel
  - Discrete Symmetries
    - Even under parity operations, forbidding the structures:

$$1 \otimes \gamma_5, \gamma_\mu \otimes \gamma_5\gamma_\mu, etc$$

    - C-parity even:

$$K^{(2)}(q_\pm, k_\pm) = \sum_n C[K_R^{(n)}(-k_\mp, -q\mp)]^T C^\dagger \otimes C[K_L^{(n)}(-k_\mp, -q_\mp)]^T C^\dagger$$

- Continuous symmetries, prominent amongst which are the vector and axial-vector Ward-Green-Takahashi (WGT) identities:

$$P_\mu \chi_\mu^{gh}(k_+, k_-) = i[S_g(k_+) - S_h(k_-)] + i(m_g - m_h)\chi_0^{gh}(k_+, k_-)$$
$$P_\mu \chi_{5\mu}^{gh}(k_+, k_-) = i[S_g(k_+)\gamma_5 + \gamma_5 S_h(k_-)] - i(m_g + m_h)\chi_5^{gh}(k_+, k_-)$$

- Decompostion of $K^{(2)}$

$$\boxed{\begin{aligned} K^{(2)} = &\left[K_{L0}^{(+)} \otimes K_{R0}^{(-)}\right] + \left[K_{L0}^{(-)} \otimes K_{R0}^{(+)}\right] \\ &+ \left[K_{L1}^{(-)} \otimes_+ K_{R1}^{(-)}\right] + \left[K_{L1}^{(+)} \otimes_+ K_{R1}^{(+)}\right] \\ &+ \left[K_{L2}^{(-)} \otimes_- K_{R2}^{(-)}\right] + \left[K_{L2}^{(+)} \otimes_- K_{R2}^{(+)}\right] \end{aligned}}$$

where $\otimes_\pm := \frac{1}{2}(\otimes \pm \gamma_5 \otimes \gamma_5)$, $\gamma_5 X^{(\pm)} \gamma_5 = \pm X^{(\pm)}$, and $\Delta^\pm_{F_{gh}} = F_g(k_+) - F_h(k_-)$.

- Deformed WTIs

$$\Sigma_B^g(k_+) = \int_{dq} \left\{ -K_{L0}^{(+)} \left[\Delta^\pm_{s_A^{gh}}(q)\right] K_{R0}^{(-)} - K_{L1}^{(-)} \left[s_B^g(q_+)\right] K_{R1}^{(-)} + K_{L1}^{(+)} \left[s_B^h(q_-)\right] K_{R1}^{(+)} \right\}, \tag{A.1a}$$

$$0 = \int_{dq} \left\{ K_{L0}^{(+)} \left[s_B^h(q_-)\right] K_{R0}^{(-)} - K_{L0}^{(-)} \left[s_B^g(q_+)\right] K_{R0}^{(+)} - K_{L2}^{(+)} \left[\Delta^\pm_{s_A^{gh}}(q)\right] K_{R2}^{(+)} \right\}, \tag{A.1b}$$

$$\Delta^\pm_{\Sigma_A^{gh}} = \int_{dq} \left\{ -K_{L0}^{(+)} \left[s_B^g(q_+)\right] K_{R0}^{(-)} + K_{L0}^{(-)} \left[s_B^h(q_-)\right] K_{R0}^{(+)} - K_{L2}^{(-)} \left[\Delta^\pm_{s_A^{gh}}(q)\right] K_{R2}^{(-)} \right\}, \tag{A.1c}$$

$$-\Sigma_B^h(k_-) = \int_{dq} \left\{ -K_{L0}^{(-)} \left[\Delta^\pm_{s_A^{gh}}(q)\right] K_{R0}^{(+)} + K_{L1}^{(-)} \left[s_B^h(q_-)\right] K_{R1}^{(-)} - K_{L1}^{(+)} \left[s_B^g(q_+)\right] K_{R1}^{(+)} \right\}, \tag{A.1d}$$

- EHM-improved kernel

$$K^{(2)} = -\mathcal{G}_{\mu\nu}(l)\gamma_\mu \otimes \gamma_\nu - \mathcal{G}_{\mu\nu}(l)$$
$$\gamma_\mu \otimes \tau_\nu(l) + \mathcal{G}_{\mu\nu}(l)\tau_\nu(l) \otimes \gamma_\mu + K_{ad}$$

$$K_{ad} = [1 \otimes_+ 1]f_{p0}^{(+)} + [-\mathcal{G}_{\mu\nu}(l)\gamma_\mu \otimes_+ \gamma_\nu]f_{p1}^{(-)}$$
$$+ [1 \otimes_- 1]f_{n0}^{(+)} + [-\mathcal{G}_{\mu\nu}(l)\sigma_{l\mu} \otimes_+ \sigma_{l\nu}]]f_{n1}^{(+)}$$

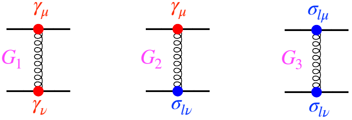

- the GMOR relation

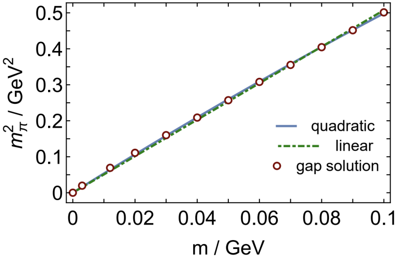

- the chiral-limit GT relation

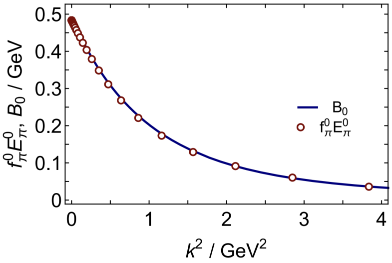

		RL	PDG	EHM-improved
π	$n=0$	0.103	0.138	0.140
	$n=1$	1.209(11)	1.3(1)	1.302(7)
K	$n=0$	0.415	0.494	0.494
	$n=1$	1.191(7)	1.460	1.440(14)
ρ	$n=0$	0.77	0.775	0.77
	$n=1$	1.140(62)	1.465(25)	1.423(48)
ϕ	$n=0$	1.049	1.020	0.926
	$n=1$	1.437(27)	1.680(20)	1.576(46)
K^*	$n=0$	0.936	0.890(14)	0.872
	$n=1$	1.298(32)	1.414(15)	1.461(22)
b_1	$n=0$	0.968	1.230(3)	1.159
	$n=1$	1.409(22)		1.671(32)
K_1^{+-}	$n=0$	1.138	1.253(7)	1.230
	$n=1$	1.458(37)	1.650(50)	1.623(30)
a_1	$n=0$	0.929	1.230(40)	1.218
	$n=1$	1.596(37)	1.655(16)	1.689(38)
K_1^{++}	$n=0$	1.123	1.403(7)	1.309
	$n=1$	1.541(12)		1.634(14)
f_0	$n=0$	0.577	$0.4-0.55$	1.237
	$n=1$	1.411(92)	$1.2-1.5$	1.96(21)
K_0^*	$n=0$	0.794	$0.63-0.73$	1.154
	$n=1$	1.439(53)	1.425(50)	2.08(22)

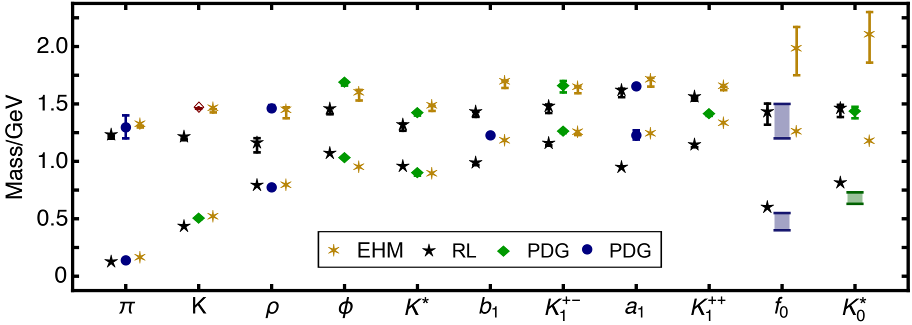
Mass/GeV
0
0.5
1.0
1.5
2.0
EHM
RL
PDG
PDG
π
K
ρ
ϕ
K^*
b_1
K_1^{+-}
a_1
K_1^{++}
f_0
K_0^*

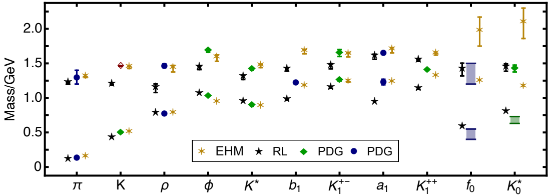

RL truncation

- mean absolute relative difference between RL masses and central experimental values is 13(8)%

EHM-improved kernel

- mean absolute relative difference: 2.9(2.7)%,✓a factor of 4.6 improvement

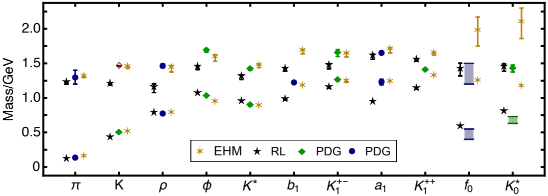

RL truncation

- mean absolute relative difference between RL masses and central experimental values is 13(8)%
- qualitative & quantitative discrepancies:
  - Ordering of $(m_{\pi'}, m_{K'})$, $(m_{\rho'}, m_{\pi'})$,$(m_{\rho'}, m_{K^{*\prime}})$: opposite to empirical ordering
  - Mass splitting $a_1 - \rho$, $b_1 - \rho$: 1/3 of empirical values; $m_{\phi'} - m_\phi$: 1/2 the expt. value.
  - Ordering K_1^{+-}, K_1^{++}: incorrect

EHM-improved kernel

- mean absolute relative difference: 2.9(2.7)%,✓a factor of 4.6 improvement
- $m_{K'} > m_{\pi'}$,$m_{\rho'} > m_{\pi'}$,$m_{\rho'} > m_{K^{*\prime}}$, ✓$a_1 - \rho$, $b_1 - \rho$ commensurate with empirical values; $m_{\phi'} - m_\phi$: matches expt. within 2%; ✓Ordering of K_1^{+-}, K_1^{++}: correct

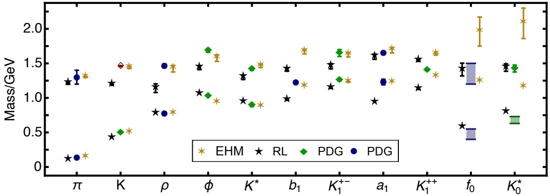

RL truncation

- mean absolute relative difference between RL masses and central experimental values is 13(8)%
- qualitative & quantitative discrepancies:
  - Ordering of $(m_{\pi'}, m_{K'})$, $(m_{\rho'}, m_{\pi'})$,$(m_{\rho'}, m_{K^{*\prime}})$: opposite to empirical ordering
  - Mass splitting $a_1 - \rho$, $b_1 - \rho$: 1/3 of empirical values; $m_{\phi'} - m_\phi$: 1/2 the expt. value.
  - Ordering K_1^{+-}, K_1^{++}: incorrect

EHM-improved kernel

- mean absolute relative difference: 2.9(2.7)%,✓a factor of 4.6 improvement
- $m_{K'} > m_{\pi'}$,$m_{\rho'} > m_{\pi'}$,$m_{\rho'} > m_{K^{*\prime}}$, ✓$a_1 - \rho$, $b_1 - \rho$ commensurate with empirical values; $m_{\phi'} - m_\phi$: matches expt. within 2%; ✓Ordering of K_1^{+-}, K_1^{++}: correct
- $m_{b_1'} = 1.67(3)$, $m_{b_1'} - m_{b_1} = 0.51(3)$ $m_{K_1^{++\prime}} = 1.63(1) m_{K_1^{++\prime}} - m_{K_1^{++}} = 0.33(1)$
- $m_{a_1'} - m_{a_1} = 0.47(4)$, $m_{K_1^{+-\prime}} - m_{K_1^{+-}} = 0.39(3)$
- $m_{b_1'} \approx m_{a_1'}$, $m_{K_1^{++\prime}} \approx m_{K_1^{+-\prime}}$

Pseudoscalar meson DFs and evolution

- DF formula for a pseudoscalar meson

$$q^\pi(x;\zeta_\mathcal{H}) = N_c \mathrm{tr} \int \frac{d^4k}{(2\pi)^4} \delta_n^x(k_\eta) \Gamma_\pi^P(k_{\bar\eta\eta};\zeta_\mathcal{H})\, S(k_{\bar\eta};\zeta_\mathcal{H}) \times \left\{ n\cdot \frac{\partial}{\partial k_\eta} \left[\Gamma_\pi^{-P}(k_{\eta\bar\eta};\zeta_\mathcal{H}) S(k_\eta;\zeta_\mathcal{H}) \right] \right\}, \tag{7}$$

- Significant features
  - canonical normalisation of the Bethe-Salpeter amplitude ensures baryon number conservation:

$$\int_0^1 dx\, q^\pi(x;\zeta_\mathcal{H}) = 1\,. \tag{8}$$

  - Owing to the symmetric character of the integrand, which ensures that neither valence degree of freedom is favoured:

$$q^\pi(x;\zeta_\mathcal{H}) = q^\pi(1-x;\zeta_\mathcal{H}) \tag{9a}$$

$$\Rightarrow \int_0^1 dx\, x q^\pi(x;\zeta_\mathcal{H}) = \tfrac{1}{2}. \tag{9b}$$

Predictions for valence DF moments

...direct calculation of the x-dependence of the valence quark DF using numerical input for the integrand functions is difficult owing to the light-front projection.

$$\langle x^m\rangle_{q^\pi}^{\zeta_{\mathcal{H}}} = \int dx x^m q^\pi(x;\zeta_{\mathcal{H}}) \tag{10a}$$

$$= \frac{N_c}{n\cdot P}\mathrm{tr}\int \frac{d^4k}{(2\pi)^4}\left[\frac{n\cdot k_\eta}{n\cdot P}\right]^m \Gamma_\pi^P(k_{\bar\eta\eta};\zeta_{\mathcal{H}})\, S(k_{\bar\eta};\zeta_{\mathcal{H}})$$

$$\times \left\{n\cdot\frac{\partial}{\partial k_\eta}\left[\Gamma_\pi^{-P}(k_{\eta\bar\eta};\zeta_{\mathcal{H}})S(k_\eta;\zeta_{\mathcal{H}})\right]\right\}, \tag{10b}$$

- $m=0$, $\langle x^0\rangle = 1$: **baryon number conservation**
- $m=1$, $\langle x^1\rangle = 1/2$: **momentum conservation** at $\zeta_{\mathcal{H}}$

Predictions for valence DF moments

moment m	π_0	π_0^{RL}	$\pi_1^{(a)}$	$\pi_1^{(b)}$	scale free
2	0.297	0.302	0.275	0.275	0.286
3	0.195	0.203	0.162	0.1625	0.179
4	0.137	0.146	0.104	0.104	0.119
5	0.102	0.109	0.0725	0.0725	0.0833
6	0.0788	0.0848	0.0541	0.0548	0.0606
7	0.0628	0.0673	0.0426	0.0444	0.0455
8	0.0513	0.0544	0.0349	0.0379	0.0350
9	0.0428	0.0446	0.0296	0.0337	0.0275
10	0.0363	0.0370	0.0256	0.0307	0.0220

- scale-free DF:

$$q^{\mathrm{sf}}(x) = 30x^2(1-x)^2. \tag{11}$$

- Ground-state pion: closely **aligned with** M. Ding, Phys. Rev. D 101(5), 054014 (2020);
- π_1 moments:
  - $\pi_1^{(a)}$: all source moments were truncated to three significant figures
  - $\pi_1^{(b)}$: $m = 3$ moment is the precise result obtained from the applicable **recursion relation** $\langle x^3\rangle_{\zeta_H} = -1/4\langle x^0\rangle_{\zeta_H} + 3/2\langle x^2\rangle_{\zeta_H}$
- **SPM extrapolations** based on moments $0 \leq m \leq 5$

Predictions for valence DF moments

moment m	π_0	π_0^{RL}	$\pi_1^{(a)}$	$\pi_1^{(b)}$	scale free
2	0.297	0.302	0.275	0.275	0.286
3	0.195	0.203	0.162	0.1625	0.179
4	0.137	0.146	0.104	0.104	0.119
5	0.102	0.109	0.0725	0.0725	0.0833
6	0.0788	0.0848	0.0541	0.0548	0.0606
7	0.0628	0.0673	0.0426	0.0444	0.0455
8	0.0513	0.0544	0.0349	0.0379	0.0350
9	0.0428	0.0446	0.0296	0.0337	0.0275
10	0.0363	0.0370	0.0256	0.0307	0.0220

- RL truncation is not reliable for excited states: fail to guarantee $(\langle x\rangle_{q^{\pi_1}}^{\zeta_{\mathcal{H}}})^2 < \langle x^2\rangle_{q^{\pi_1}}^{\zeta_{\mathcal{H}}}$ – **Cauchy-Schwarz inequality**; ..poor structural picture

Predictions for valence DF moments

moment m	π_0	$\pi_0^{\rm RL}$	$\pi_1^{(a)}$	$\pi_1^{(b)}$	scale free
2	0.297	0.302	0.275	0.275	0.286
3	0.195	0.203	0.162	0.1625	0.179
4	0.137	0.146	0.104	0.104	0.119
5	0.102	0.109	0.0725	0.0725	0.0833
6	0.0788	0.0848	0.0541	0.0548	0.0606
7	0.0628	0.0673	0.0426	0.0444	0.0455
8	0.0513	0.0544	0.0349	0.0379	0.0350
9	0.0428	0.0446	0.0296	0.0337	0.0275
10	0.0363	0.0370	0.0256	0.0307	0.0220

- RL truncation is not reliable for excited states: fail to guarantee $(\langle x\rangle_{q^{\pi_1}}^{\zeta_{\mathcal{H}}})^2 < \langle x^2\rangle_{q^{\pi_1}}^{\zeta_{\mathcal{H}}}$ – **Cauchy-Schwarz inequality**; ..poor structural picture
- Signals for pointwise DF reconstruction
  - π_0 moments: uniformly larger than those of $q^{\rm sf}$, indicating **dilation** and a **lower peak**.
  - low-m π_1 moments: smaller..., should be **narrower** and **taller** on $x \simeq 1/2$
  - large-m π_1 moments: exhibit **greater support** on the endpoint domains

DF reconstruction

In studies of pseudoscalar meson valence-quark DFs that incorporate the ultraviolet behaviour of the pion wave function prescribed by QCD

$$q^{\pi}(x;\zeta_{\mathcal{H}}) \overset{x\simeq 1}{\approx} (1-x)^2, \tag{12}$$

DF reconstruction

In studies of pseudoscalar meson valence-quark DFs that incorporate the ultraviolet behaviour of the pion wave function prescribed by QCD

$$q^{\pi}(x;\zeta_{\mathcal{H}}) \overset{x\simeq 1}{\approx} (1-x)^2, \tag{12}$$

- Ground state pion

$$q^{\pi_0}(x;\zeta_{\mathcal{H}}) = n_\pi \ln[1 + x^2(1-x)^2/\rho_\pi^2] \\ =: \tilde{q}(x;\zeta_{\mathcal{H}})\,, \tag{13}$$

– flexible enough to reflect EHM-induced dilation and QCD-consistent endpoint behavior

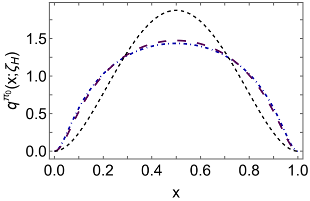

Figure: Long-dashed purple curve – EHM-improved bound-state kernels; dot-dashed blue curve – RL result. Dashed black curve - scale-free DF.

	π_0	π_0^{RL}	$\pi_1^{(a)}$	$\pi_1^{(b)}$
$\overline{\mathrm{ard}}$	1.7(8)	4.1(1.4)	1.4(1.0)	5.0(2.8)
ρ	0.0750	0.0613	0.743	0.663
a_2	0	0	0.116	0.191
a_4	0	0	0.441	0.487
a_6	0	0	−0.00300	0.0684

DF reconstruction

In studies of pseudoscalar meson valence-quark DFs that incorporate the ultraviolet behaviour of the pion wave function prescribed by QCD

$$q^{\pi}(x;\zeta_{\mathcal{H}}) \overset{x\simeq 1}{\approx} (1-x)^2, \tag{12}$$

- Ground state pion

$$\begin{aligned} q^{\pi_0}(x;\zeta_{\mathcal{H}}) &= n_\pi \ln[1 + x^2(1-x)^2/\rho_\pi^2] \\ &=: \tilde{q}(x;\zeta_{\mathcal{H}})\,, \end{aligned} \tag{13}$$

– flexible enough to reflect EHM-induced dilation and QCD-consistent endpoint behavior

- **least-squares fit**;

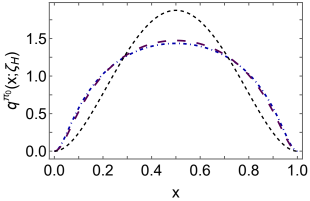

Figure: Long-dashed purple curve – EHM-improved bound-state kernels; dot-dashed blue curve – RL result. Dashed black curve - scale-free DF.

	π_0	π_0^{RL}	$\pi_1^{(a)}$	$\pi_1^{(b)}$
$\overline{\mathrm{ard}}$	1.7(8)	4.1(1.4)	1.4(1.0)	5.0(2.8)
ρ	0.0750	0.0613	0.743	0.663
a_2	0	0	0.116	0.191
a_4	0	0	0.441	0.487
a_6	0	0	−0.00300	0.0684

DF reconstruction

In studies of pseudoscalar meson valence-quark DFs that incorporate the ultraviolet behaviour of the pion wave function prescribed by QCD

$$q^{\pi}(x;\zeta_{\mathcal{H}}) \overset{x\simeq 1}{\approx} (1-x)^2, \tag{12}$$

- Ground state pion

$$q^{\pi_0}(x;\zeta_{\mathcal{H}}) = n_\pi \ln[1 + x^2(1-x)^2/\rho_\pi^2]$$
$$=: \tilde{q}(x;\zeta_{\mathcal{H}})\,, \tag{13}$$

– flexible enough to reflect EHM-induced dilation and QCD-consistent endpoint behavior

  - **least-squares fit**;
  - similar across kernels, showing clear **dilation** from the scale-free profile.

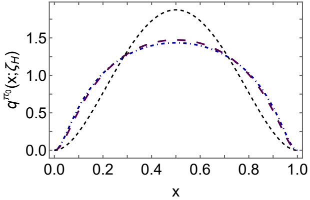

Figure: Long-dashed purple curve – EHM-improved bound-state kernels; dot-dashed blue curve – RL result. Dashed black curve - scale-free DF.

	π_0	π_0^{RL}	$\pi_1^{(a)}$	$\pi_1^{(b)}$
$\overline{\mathrm{ard}}$	1.7(8)	4.1(1.4)	1.4(1.0)	5.0(2.8)
ρ	0.0750	0.0613	0.743	0.663
a_2	0	0	0.116	0.191
a_4	0	0	0.441	0.487
a_6	0	0	-0.00300	0.0684

DF reconstruction

- Lightest pion radial excitation

$$q^{\pi_1}(x;\zeta_{\mathcal{H}}) = \tilde{q}(x;\zeta_{\mathcal{H}})\left[1 + \sum_{i=1,2,3} a_{2i} C_{2i}^{3/2}(1-2x)\right], \quad (14)$$

$C_n^{3/2}$: Gegenbauer polynomial of order 3/2;
ρ_{π_1}, $\{a_{2i}\}$: reconstruction parameters

DF reconstruction

- Lightest pion radial excitation

$$q^{\pi_1}(x;\zeta_{\mathcal{H}}) = \tilde{q}(x;\zeta_{\mathcal{H}})\left[1+\sum_{i=1,2,3} a_{2i}C_{2i}^{3/2}(1-2x)\right], \quad (14)$$

$C_n^{3/2}$: Gegenbauer polynomial of order 3/2;
ρ_{π_1}, $\{a_{2i}\}$: reconstruction parameters

  - **least-squares fit**, but with an added **non-negativity constraint** to avoid unphysical oscillations.

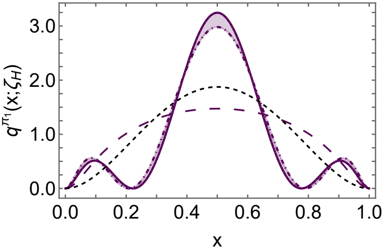

Figure: Solid purple curve - $\pi_1^{(a)}$; dot-dashed purple curve – $\pi_1^{(b)}$; long-dashed purple - π_0; dashed black - scale-free DF.

	π_0	π_0^{RL}	$\pi_1^{(a)}$	$\pi_1^{(b)}$
ard	1.7(8)	4.1(1.4)	1.4(1.0)	5.0(2.8)
ρ	0.0750	0.0613	0.743	0.663
a_2	0	0	0.116	0.191
a_4	0	0	0.441	0.487
a_6	0	0	-0.00300	0.0684

- Lightest pion radial excitation

$$q^{\pi_1}(x;\zeta_{\mathcal{H}}) =$$
$$\tilde{q}(x;\zeta_{\mathcal{H}})\left[1+\sum_{i=1,2,3} a_{2i}C_{2i}^{3/2}(1-2x)\right], \quad (14)$$

$C_n^{3/2}$: Gegenbauer polynomial of order 3/2;
ρ_{π_1}, $\{a_{2i}\}$: reconstruction parameters

  - **least-squares fit**, but with an added **non-negativity constraint** to avoid unphysical oscillations.
  - Only the **EHM-improved kernels** provide meaningful results for π_1.

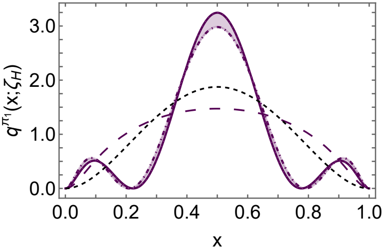

Figure: Solid purple curve - $\pi_1^{(a)}$; dot-dashed purple curve – $\pi_1^{(b)}$; long-dashed purple - π_0; dashed black - scale-free DF.

	π_0	π_0^{RL}	$\pi_1^{(a)}$	$\pi_1^{(b)}$
ard	1.7(8)	4.1(1.4)	1.4(1.0)	5.0(2.8)
ρ	0.0750	0.0613	0.743	0.663
a_2	0	0	0.116	0.191
a_4	0	0	0.441	0.487
a_6	0	0	−0.00300	0.0684

- Lightest pion radial excitation

$$q^{\pi_1}(x;\zeta_{\mathcal{H}}) = \tilde{q}(x;\zeta_{\mathcal{H}})\left[1 + \sum_{i=1,2,3} a_{2i} C_{2i}^{3/2}(1-2x)\right], \quad (14)$$

$C_n^{3/2}$: Gegenbauer polynomial of order 3/2;
ρ_{π_1}, $\{a_{2i}\}$: reconstruction parameters

- **least-squares fit**, but with an added **non-negativity constraint** to avoid unphysical oscillations.
- Only the **EHM-improved kernels** provide meaningful results for π_1.
- The two reconstructions (using two moment sets) are **qualitatively identical**, with small quantitative difference reflecting uncertainties in true moments.

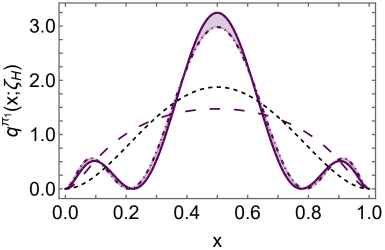

Figure: Solid purple curve - $\pi_1^{(a)}$; dot-dashed purple curve – $\pi_1^{(b)}$; long-dashed purple - π_0; dashed black - scale-free DF.

	π_0	π_0^{RL}	$\pi_1^{(a)}$	$\pi_1^{(b)}$
ard	1.7(8)	4.1(1.4)	1.4(1.0)	5.0(2.8)
ρ	0.0750	0.0613	0.743	0.663
a_2	0	0	0.116	0.191
a_4	0	0	0.441	0.487
a_6	0	0	−0.00300	0.0684

Three-peak structure

- $x = 1/2$ peak: much narrower and taller than the analogous feature of the **scale-free DF**
- Secondary peaks at $x \sim 0.1$ and $x \sim 0.9$, with minima near $x \sim 0.2, 0.8$
- These features explains:
    - **Smaller low**-m moments than scale-free DF (due to central peak)
    - **Larger hign**-m moments (due to enhanced endpoint support)

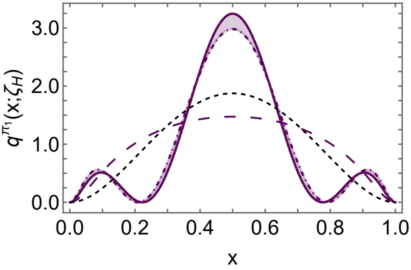

Figure: Hadron-scale valence DFs in the lightest pion radial excitation.

DFs beyond the hadron scale

- At the hadron scale $\zeta_{\mathcal{H}}$, valence degrees of freedom carry all properties of a given hadron
  - All glue and sea partonic Fock space components are sublimated into the valence degrees of freedom at $\zeta_{\mathcal{H}}$ via dressing.
- As the resolving scale increases ($\zeta > \zeta_H$), glue and sea DFs become nonzero.
  - This behavior is governed by **DGLAP evolution equations**, implemented here via the **All-Orders (AO) scheme**.
- The hadron scale is naturally defined by the process-independent effective charge: $\zeta_{\mathbf{H}} = \mathbf{0.331(2)}$ GeV. – consistent with lattice QCD: $\zeta_{\mathbf{H}} = \mathbf{0.350(44)}$ GeV.

  Z.-F. Cui et al., Chin. Phys. C 44, 083102 (2020)
  Y. Lu et al., Phys. Lett. B 850, 138534 (2024)

DFs beyond the hadron scale

Using lQCD, an exploratory effort was made to identify differences between $\pi_{0,1}$ valence quark structure at $\zeta_3 = 3.2\,\text{GeV}$. X. Gao et al., Phys. Rev. D 103(9), 094510 (2021)

- After AO evolution to ζ_3, the differences between π and π_1 valence DFs are **reduced**.
- The absolute minima in the π_1 DF have become **diffuse regions** containing an **inflection point**.

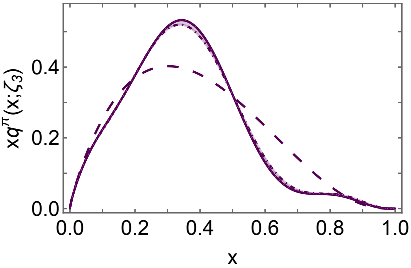

Figure: Valence quark DFs in the pion and its first radial excitation, at resolving scale $\zeta_3 = 3.2\,\text{GeV}$. Long-dashed – π_0; dot-dashed – $\pi_1^{(b)}$; solid curve –$\pi_1^{(a)}$.

DFs beyond the hadron scale

Using lQCD, an exploratory effort was made to identify differences between $\pi_{0,1}$ valence quark structure at $\zeta_3 = 3.2\,\text{GeV}$. X. Gao et al., Phys. Rev. D 103(9), 094510 (2021)

- After AO evolution to ζ_3, the differences between π and π_1 valence DFs are **reduced**.
- The absolute minima in the π_1 DF have become **diffuse regions** containing an **inflection point**.
- Differences remain discernible to precision measurements + phenomenological analysis.
- π_1 targets (real/virtual) are unlikely to ever be achievable $\rightarrow$ direct measurements improbable.
- Nevertheless, our predictions serve as benchmarks for pion and radial excitation studies.

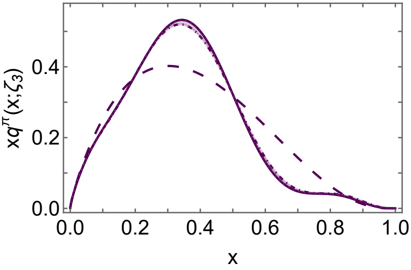

Figure: Valence quark DFs in the pion and its first radial excitation, at resolving scale $\zeta_3 = 3.2\,\text{GeV}$. Long-dashed – π_0; dot-dashed – $\pi_1^{(b)}$; solid curve –$\pi_1^{(a)}$.

DFs beyond the hadron scale

Table: Selected Mellin moments of $\pi_{0,1}$ DFs – valence ($\mathcal{V}$), glue ($\mathcal{g}$), and flavour separated sea ($\mathcal{S}$) – all determined at the scale $\zeta_3 = 3.2$ GeV.

	π_0	$\pi_1^{(a)}$	$\pi_1^{(b)}$
$\mathcal{V}$ $\langle x\rangle_{q^\pi}^{\zeta_3}$	0.220	0.220	0.220
$\langle x^2\rangle_{q^\pi}^{\zeta_3}$	0.0831	0.0772	0.0779
$\langle x^3\rangle_{q^\pi}^{\zeta_3}$	0.0397	0.0334	0.0341
$\langle x^4\rangle_{q^\pi}^{\zeta_3}$	0.0218	0.0167	0.0173
$\mathcal{g}$ $\langle x\rangle_{g^\pi}^{\zeta_3}$	0.434	0.434	0.434
$\langle x^2\rangle_{g^\pi}^{\zeta_3}$	0.0346	0.0321	0.0324
$\mathcal{S}$ $\langle x\rangle_{u^\pi}^{\zeta_3}$	0.0372	0.0372	0.0372
$\langle x\rangle_{s^\pi}^{\zeta_3}$	0.0308	0.0308	0.0308
$\langle x\rangle_{c^\pi}^{\zeta_3}$	0.0187	0.0187	0.0187
$\langle x^2\rangle_{u^\pi}^{\zeta_3}$	0.00274	0.00254	0.00257
$\langle x^2\rangle_{s^\pi}^{\zeta_3}$	0.00219	0.00204	0.00206
$\langle x^2\rangle_{c^\pi}^{\zeta_3}$	0.00117	0.00109	0.00110

- Evolution does not alter the relative sizes of ground-state vs. radial excitation moments.

DFs beyond the hadron scale

- We compare the distributions for π_0 **(long dashed)** and π_1 **(solid curve)**.

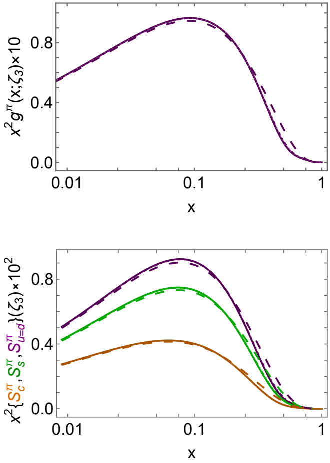

Figure: Panel A. Glue DFs in the pion (long dashed) and its first radial excitation (solid curve). Panel B. Analogous sea quark DFs.)

Glue and sea DFs differ slightly between π_0 and π_1, but remain phenomenologically indistinguishable.

- We compare the distributions for π_0 **(long dashed)** and π_1 **(solid curve)**.
- The ground-state DFs possess a small but noticeable amount of **additional support** on $0.25 \lesssim x \lesssim 0.75$.

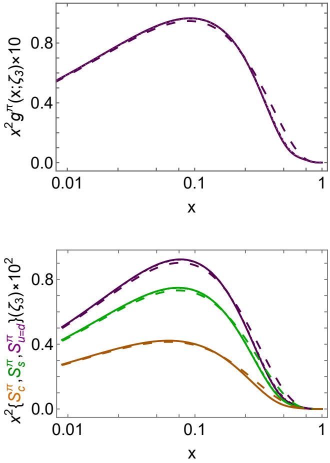

Figure: Panel A. Glue DFs in the pion (long dashed) and its first radial excitation (solid curve). Panel B. Analogous sea quark DFs.)

Glue and sea DFs differ slightly between π_0 and π_1, but remain phenomenologically indistinguishable.

- We compare the distributions for π_0 **(long dashed)** and π_1 **(solid curve)**.
- The ground-state DFs possess a small but noticeable amount of **additional support** on $0.25 \lesssim x \lesssim 0.75$.
- However, even if π_1 DFs were accessible via structure function measurements, the differences are **too small to be empirically discernible**.
- These results still serve as reference points for other theoretical analyses.

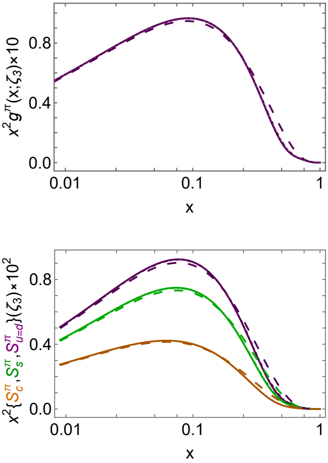

Figure: Panel A. Glue DFs in the pion (long dashed) and its first radial excitation (solid curve). Panel B. Analogous sea quark DFs.)

Glue and sea DFs differ slightly between π_0 and π_1, but remain phenomenologically indistinguishable.

Summary

- We computed valence, glue, and four-flavour sea DFs for π_0 and π_1 using a symmetry-preserving CSM framework.
  - The kernels incorporate nonperturbative improvements to the leading-order bound-state equations, particularly including ACM.
  - crucial to obtaining a plausible description of the structure of the pion radial excitation.

Summary

- We computed valence, glue, and four-flavour sea DFs for π_0 and π_1 using a symmetry-preserving CSM framework.
  - The kernels incorporate nonperturbative improvements to the leading-order bound-state equations, particularly including ACM.
  - crucial to obtaining a plausible description of the structure of the pion radial excitation.
- The π_1 valence DF at $\zeta_{\mathcal{H}}$ exhibits a distinct three-peak structure, consistent with expectations from a radially excited wave function.
- Mellin moment analysis shows:
  - π_0 moments are larger than π_1 for $m \geq 2$.
  - π_1 moments are smaller than the scale-free DF for $m = 2$–7, but become larger for $m \geq 8$.

Summary

- We computed valence, glue, and four-flavour sea DFs for π_0 and π_1 using a symmetry-preserving CSM framework.
  - The kernels incorporate nonperturbative improvements to the leading-order bound-state equations, particularly including ACM.
  - crucial to obtaining a plausible description of the structure of the pion radial excitation.
- The π_1 valence DF at $\zeta_{\mathcal{H}}$ exhibits a distinct three-peak structure, consistent with expectations from a radially excited wave function.
- Mellin moment analysis shows:
  - π_0 moments are larger than π_1 for $m \geq 2$.
  - π_1 moments are smaller than the scale-free DF for $m = 2$–7, but become larger for $m \geq 8$.
- Our predictions can serve as valuable benchmarks for other theory attempts to expose structural features of the pion and its radial excitations.

DFs in lQCD: comments (Back-up)

- Using lQCD, an exploratory effort was made to identify differences between $\pi_{0,1}$ valence quark structure at $\zeta_3 = 3.2\,\text{GeV}$. X. Gao et al., Phys. Rev. D 103(9), 094510 (2021)
- We use this scale hereafter in comparing valence, glue and sea DFs in these systems.
- LQCD study reported: $m = 1, 2, 3, 4$: in all cases, $\langle x^m \rangle_{q^{\pi_1}}^{\zeta_3} > \langle x^m \rangle_{q^{\pi_0}}^{\zeta_3}$.
– incompatible with our results
- It is necessary for additional lQCD analyses to be completed before it becomes possible to judge the potential of the lattice approach to deliver reliable information on excited-state DFs

DSE: Interaction

- Qin-Chang Interaction [Qin:2011xq][Binosi:2014aea]

$$\tilde{\mathcal{G}}(y) = \frac{8\pi^2 D}{\omega^4} e^{-y/\omega^2} + \frac{8\pi^2 \gamma_m \mathcal{F}(y)}{\ln\left[\tau + \left(1 + y/\Lambda^2_{\mathrm{QCD}}\right)^2\right]},$$

where $\gamma_m = 4/\beta_0$, $\beta_0 = 25/3$, $\Lambda_{QCD} = 0.234\ \mathrm{GeV}$, $\ln(\tau + 1) = 2$, and $\mathcal{F}(y) = \{1 - exp(-y/[4m_t^2])\}/y$.

DSE: Interaction

- Qin-Chang Interaction [Qin:2011xq][Binosi:2014aea]

$$\tilde{\mathcal{G}}(y) = \frac{8\pi^2 D}{\omega^4} e^{-y/\omega^2} + \frac{8\pi^2 \gamma_m \mathcal{F}(y)}{\ln\left[\tau + \left(1 + y/\Lambda^2_{\rm QCD}\right)^2\right]},$$

where $\gamma_m = 4/\beta_0$, $\beta_0 = 25/3$, $\Lambda_{QCD} = 0.234\ \mathrm{GeV}$, $\ln(\tau + 1) = 2$, and $\mathcal{F}(y) = \{1 - exp(-y/[4m_t^2])\}/y$.

  - $0 < \tilde{\mathcal{G}}(0) < \infty$ A nonzero gluon mass-scale appears as a consequence of EHM in QCD.

DSE: Interaction

- Qin-Chang Interaction [Qin:2011xq][Binosi:2014aea]

$$\tilde{\mathcal{G}}(y) = \frac{8\pi^2 D}{\omega^4} e^{-y/\omega^2} + \frac{8\pi^2 \gamma_m \mathcal{F}(y)}{\ln\left[\tau + \left(1 + y/\Lambda^2_{\mathrm{QCD}}\right)^2\right]},$$

where $\gamma_m = 4/\beta_0$, $\beta_0 = 25/3$, $\Lambda_{QCD} = 0.234\ \mathrm{GeV}$, $\ln(\tau + 1) = 2$, and $\mathcal{F}(y) = \{1 - exp(-y/[4m_t^2])\}/y$.

  - $0 < \tilde{\mathcal{G}}(0) < \infty$ A nonzero gluon mass-scale appears as a consequence of EHM in QCD.
  - The large-momentum behaviour ensures that the one-loop renormalisation group flow of QCD is preserved.